An experimental study of reverse compound lean in a linear turbine cascade

D A Bagshaw[1], **G L Ingram**[1], **D G Gregory-Smith**[1]*, and **M R Stokes**[2]
[1]School of Engineering, University of Durham, UK
[2]Rolls-Royce plc, Derby, UK

Abstract: This paper describes a detailed experimental investigation into the effects of reverse compound lean (RCL) in a highly loaded axial turbine cascade. The geometry was designed using fully three-dimensional viscous CFD calculations to achieve a reduction in secondary flow. Traverses were made upstream and downstream with three-hole and five-hole probes to quantify the effects on the flow and losses produced by the leaned blade compared with a prismatic blade. These measurements were supplemented with blade static pressure measurements and surface flow visualization. It was found that the RCL blade produced higher overturning at the end-wall accompanied by higher secondary loss but this was constrained closer to the end-wall. Near mid-span, the turning was reduced slightly but the overall turning for the row was unaltered. The mid-span showed much less loss, so that overall the loss was reduced by 11 per cent. An understanding of these effects may be gained by consideration of the three-dimensional effects produced by the RCL.

Keywords: turbine blades, secondary flow, blade lean, dihedral experiment

1 INTRODUCTION

This paper describes a detailed experimental investigation into the effects of reverse compound lean (RCL) in a highly loaded axial turbine cascade. Positive compound lean (where the blade suction surface (SS) makes an obtuse angle with the end-wall) has a substantial body of literature describing it but there is much less information on the operation of RCL (where the blade SS makes an acute angle with the end-wall). Compound lean (as defined in Harrison [1]) is where the SS makes an obtuse angle with the end-wall and its shape, when viewed axially, is convex on the pressure surface. Reverse compound lean is the reverse of this and gives a concave pressure surface.

The RCL shown in this paper is achieved by fixing the end-wall section locations and varying the stacking line in between them. The geometry was designed using fully three-dimensional viscous CFD calculations to achieve a reduction in secondary flow. The experimental results comprise pneumatic probe measurements, surface flow visualization, and surface static pressures. A feature of the present work is that great care has been taken to achieve repeatable results in a similar manner to Ingram and Gregory-Smith [2]; the loss changes involved are small and careful measurement is required. Each measurement on the leaned geometry is accompanied by a measurement on the prismatic blades, thus all the measurements in this paper are new and are not simply referenced from previous studies on the 'Durham cascade'.

The aim of this work is to achieve an understanding of three-dimensional blade design, in general, and RCL, in particular, by providing a substantial body of high-quality experimental data and comparing it to other authors' studies.

2 BACKGROUND

A number of researchers have investigated the effect of lean on the flow field in axial flow turbines, for

---

Corresponding author: School of Engineering, University of Durham, South Road, Durham DH1 1LE, UK.

example, those of Sharma *et al.* [3] and Harrison [1]. A review of the three-dimensional design of aerofoils, which includes blade lean was undertaken by Denton and Xu [4].

Sharma *et al.* [3] obtained a number of results from both a linear cascade and CFD, including work on RCL. The authors demonstrated that blade lean in either direction redistributed loss. RCL reduced loss at mid-span but increased it at the end-wall, whereas compound lean demonstrated an increased loss at the mid-span region and a reduction towards the end-walls.

The work of Harrison [1] is based on experimental results of a linear cascade. Harrison investigated three blade stacking arrangements, a prismatic reference case, a straight leaned case, and a compound leaned one. The surface static pressures for the compound leaned blade showed a behaviour similar to the work of Sharma *et al.* [3].

The work of Denton and Xu [4] includes, among other three-dimensional effects, tangential lean. The paper derives a qualitative relationship between the lean-induced blade forces, the radial pressure gradient, and the streamline curvature acceleration. It is noted that for low aspect ratio blades (like the Durham cascade), the radial pressure term dominates and hence 'the radial blade force will be opposed mainly by the increased radial pressure gradient'.

In general, all researchers obtain similar flow behaviours, but the benefits of the leaning, that is, loss reduction and exit yaw angle distribution seem to vary depending on the inlet flow and geometry.

3 BLADE DESIGN

A series of CFD tests were conducted to investigate the effects of different degrees of compound lean. The final choice was made on the basis of a predicted significant effect of lean and reduction in secondary flow. In addition, the design had to be reasonably realistic for engine application with a modest degree of compound lean. The geometry chosen for investigation was an elliptical tangential stacking profile with $15°$ inclination at the end-wall. A schematic of the prismatic and leant blade is shown in Fig. 1(a) and the geometry is shown in Fig. 1(b), this geometry was called the C1 blade. To ensure direct comparison between the prismatic and RCL blades, the geometry was chosen to have the same overall turning and blade profile.

4 EXPERIMENTAL TECHNIQUE

The so-called 'Durham cascade' is a linear cascade of six blades each of 400 mm span. It is a well-known CFD test case [5]. Upstream of the test section is a
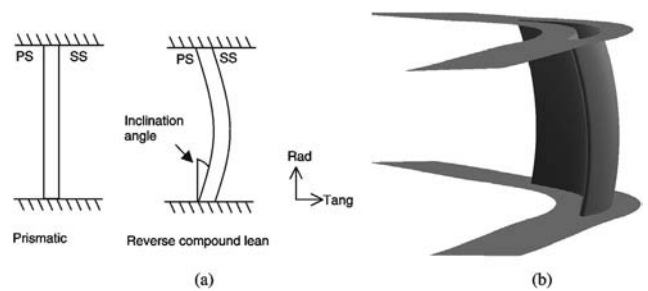

Fig. 1 Schematic (a) and geometry (b) of RCL

turbulence grid which generates a 4 per cent inlet turbulence intensity. There is also a boundary layer bleed on one side of the tunnel, which introduces an asymmetry into the inlet conditions with a corresponding asymmetry in the exit flow. The inlet flow conditions are shown in Fig. 2, which shows the asymmetry in the inlet flow. The measurements are taken from slots cut into the cascade on the 'upper' ($r = 400$ mm) wall which means that the readings taken near this wall will be much less accurate, due to leakage through the slots and the effect of the probe stem.

The original prismatic blades (described in this paper as the C0 blade) were measured in a 'back-to-back' method with the C1 blades to provide an accurate comparison of loss changes, as described by Ingram and Gregory-Smith [2].

Pneumatic probe measurements used conventional three- and five-hole probes. Manufacture of the C1 blade using sterolithography allowed pressure tappings to be placed along the span of the blade. For each probe type (five-hole and three-hole) and each geometry (C0 and C1), three sets of readings were taken, but with a reset of the measurement system between each measurement run. As the prismatic blade profile is already quite efficient, the loss changes were very small and this technique gives confidence that the changes in loss are greater than the errors in the measurement system.
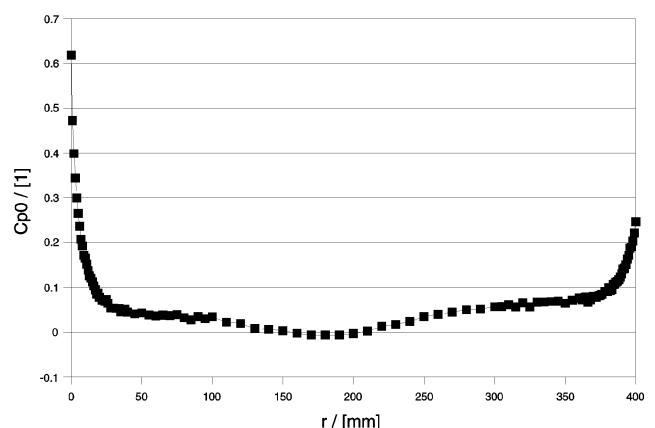

Fig. 2 Inlet boundary layer

Flow visualization was conducted using a two colour oil–dye mixture applied to the surface of the blade. For a detailed description of both the cascade and the experimental technique, see reference [6]. The major difference in experimental technique between this work and earlier tests in the Durham cascade is that the full 400 mm span is measured rather than just half span.

5 AREA TRAVERSES

A measurement plane 28 per cent of the blade axial chord (Cax) downstream of the trailing edges was used. All the area traverses were conducted over the full span of the cascade but some results are presented for only the 'lower' half of the cascade (0–200 mm). This is because the effects are similar at both ends of the cascade and the measurements at the 'lower' half of the cascade are more accurate for reasons discussed earlier.

Experimental loss contours for the C0 and C1 blades are given in Fig. 3. The mean of the three data sets for the five- and three-hole probes are combined to give a complete passage loss distribution. Each contour plot, therefore, represents the results of some six separate traverses. The combined dataset was only for the loss as the three-hole probe data cannot give pitch angles and therefore neither secondary velocities nor secondary kinetic energy. The following points can be determined from an inspection of Fig. 3.

1. The reverse compound leaned blades, C1, produce a noticeably bowed wake.
2. The mid-span of the C1 wake has a slightly lower peak loss than that of the prismatic blades, Cp0 of 0.5 compared with 0.6.
3. The corner vortex loss core (seen at −320 mm tangential, 5 mm radial for C0) is shifted tangentially

(relative to the wake) in C1. This is due to increased overturning at the wall.
4. The trailing vorticity/SS horseshoe-vortex (SS HSV) loss core is much weaker in the C1 blades. Where as previously (in C0) this loss was clearly defined and separate; here, the region appears to have merged with the passage vortex core (located at −250 mm tangential, 60 mm radial).
5. The passage vortex loss core has itself increased in strength for the C1 blades and this is partly due to combining the loss from the SS HSV core and partly to increased loss generation in the secondary flows.
6. There is a slight movement of the secondary losses toward the end-wall. The passage vortex loss feature is in a similar position in both C0 and C1. Only the decrease in strength of the trailing vorticity/SS HSV loss core has brought about any apparent shift in loss.

The secondary velocity vectors for the C0 and C1 blades are given in Fig. 4. The definition of secondary vectors used in this paper is given in Appendix 2. The secondary vectors were obtained from the mean of the five-hole probe traverses; therefore each vector plot represents three separate measurement traverses. Figure 4 shows the following.

1. The SS HSV vectors are weaker in C1 than C0 and this leads to a weaker interaction with the passage vortex.
2. The passage vortex is similar in size and strength for C0 and C1, but has shifted slightly radially toward the end-wall.
3. The near-wall region for the C1 blade has strong secondary velocities, associated with increased overturning. The corner vortex is more difficult to discern in C1 due to this strong overturning.
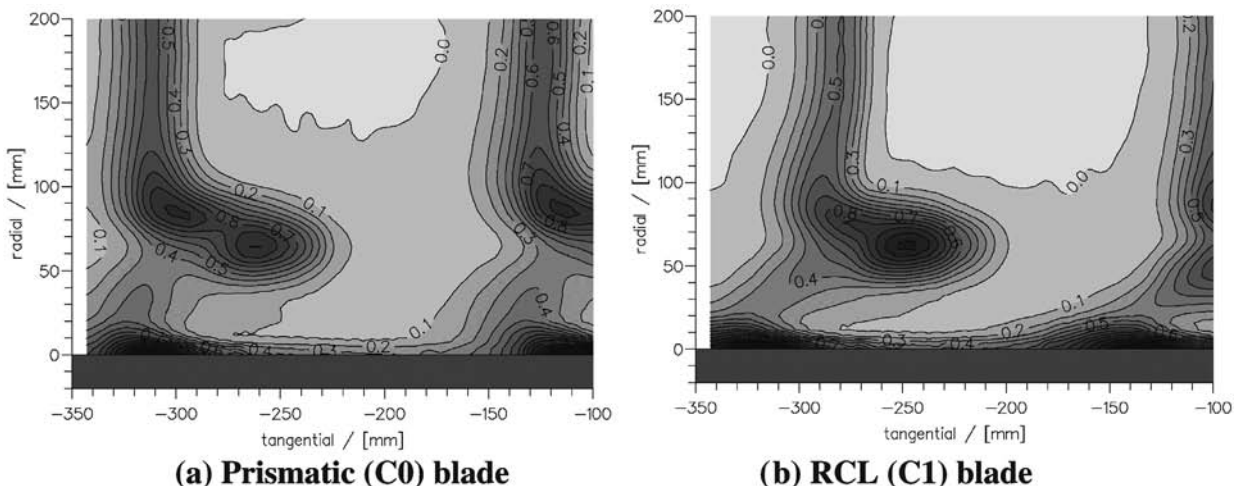

(a) Prismatic (C0) blade   (b) RCL (C1) blade

Fig. 3 Loss contours at 28 per cent Cax downstream

(a) Prismatic (C0) blade   (b) RCL (C1) blade
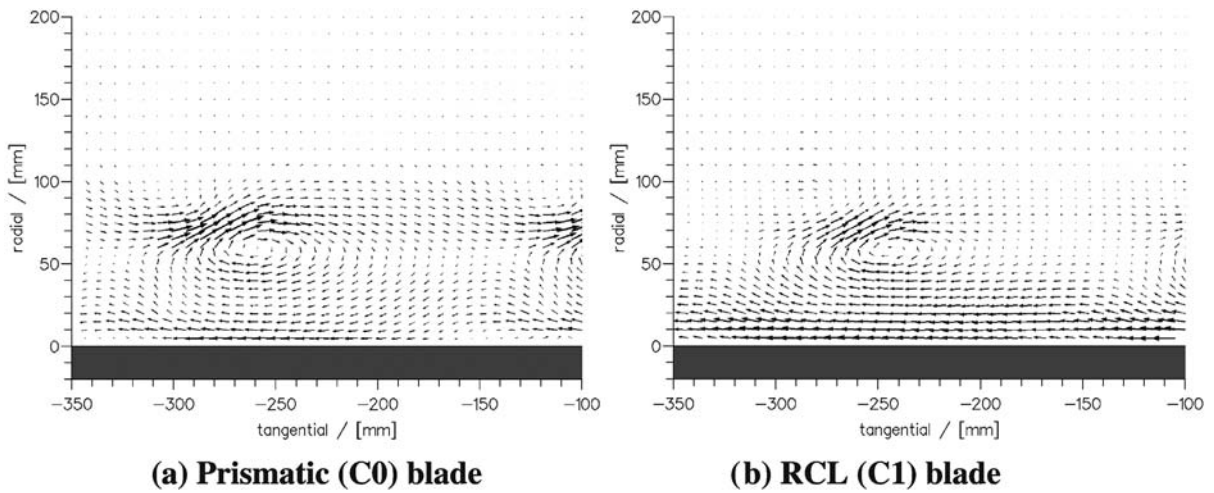
Fig. 4   Secondary vectors at 28 per cent Cax downstream

6   PITCH-AVERAGED RESULTS

The repeatability of the traverse data is shown in Fig. 5, where the pitch-averaged loss coefficient for each of the three traverses for C0 and C1 are plotted. The differences between different runs on the same geometry are much smaller than the differences between geometries, giving confidence that the results presented in this paper are reliable. Figure 6 shows a similar plot for pitch-averaged yaw angle; again the repeatability is very good except for one traverse for C1 which shows an offset between it and the other two C1 runs. This offset was put down to an error in setting the yaw angle on the five-hole probe before traversing.

The pitch-averaged results give a quantitative view of Figs 3 and 4. The pitch-averaged graphs show that the asymmetry in the inlet boundary layer convects through the passage for both the prismatic and leaned geometries. The slot in the end-wall through which the cobra-headed probe is traversed also introduces asymmetry into the measured flow field. The loss cores in Fig. 5 are of different size and

there was more underturning (Fig. 6) on the lower side (0–200 mm) for both C0 and C1.

Having established the repeatability of the traversing from Figs 5 and 6, the following key points about the differences between C0 and C1 can be established.

1. There is a slight radial shift towards the end-wall of the loss core associated with the passage vortex.
2. The peak loss of the passage vortex core also increased in the experimental result for C1.
3. There is a reduction in mid-span loss for C1 compared with C0.
4. The near-wall loss is higher for C1 than that for C0. This is not clear when looking at the area plots but is highlighted in the pitch-averaged data.
5. There is reduced turning at mid-span for the C1 geometry. Therefore, the C1 blade is unloaded at mid-span compared with the prismatic case.
6. The new blades increase the overturning at the wall while maintaining a similar level of underturning. Therefore, the C1 blade is more highly loaded at the ends.
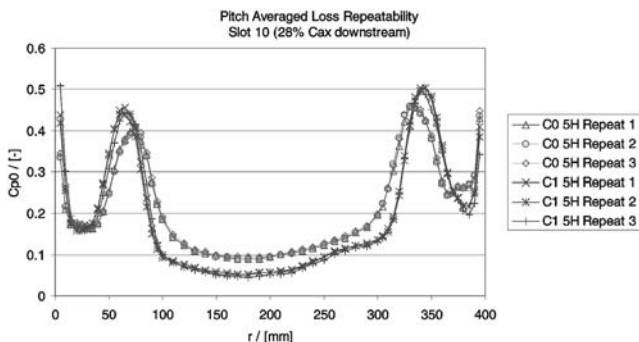

Fig. 5   Repeated pitch-averaged loss measurements at 28 per cent Cax downstream
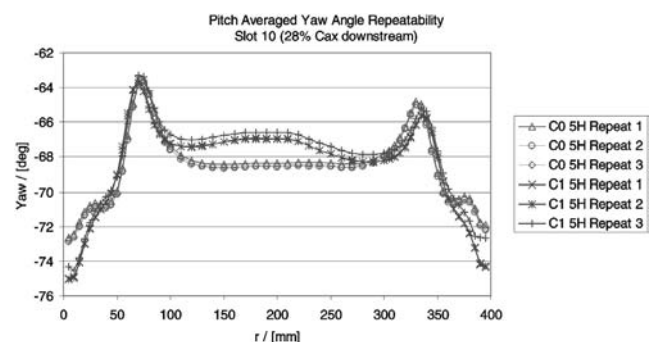

Fig. 6   Pitch-averaged yaw angle at 28 per cent Cax downstream

Table 1 Area-averaged net loss 28 per cent Cax downstream

	Area averaged loss (Cp0)		Prismatic (%)	
	C0	C1	C0	C1
Total	0.1911	0.1707	100.0	89.3
Mid-span	0.0921	0.0533	100.0	57.9
Secondary	0.0990	0.1174	100.0	118.6

7 AREA MASS-AVERAGED RESULTS

Table 1 shows area-averaged loss coefficients for the lower half of the span (0–200 mm) and so excludes the inaccuracies near the upper wall. They are net values having the inlet loss subtracted and so represent the loss growth through the cascade. Mid-span loss is defined as the area-averaged loss between 180 and 200 mm in the radial direction. Secondary loss is simply the total loss minus the mid-span loss.

Table 1 shows an overall reduction of loss for the C1 geometry with an increase in secondary loss and a reduction in mid-span loss.

The results for the three- and five-hole probes are shown as a combined loss value. The three-hole probe was traversed 0–15 mm radially, the five-hole probe was traversed 5–395 mm radially. This provides an overlap of the data and for the combined dataset, the two traverses were joined at 10 mm spanwise position. This position was chosen to ensure the maximum use of the five-hole probe while eliminating errors due to the close proximity of the five-hole probe with the wall.

The overall differences in averaged yaw angle are small; in the 5–200 mm region, the C0 area averaged yaw angle is $-68.75°$ and the C1 area-averaged yaw angle is $-68.45°$. By looking at Fig. 6, it should be noted that the average angle is in effect a mass-averaged tangent. The difference of $\sim 0.3°$ is extremely small, although larger than the accuracy of the experimental measurement system [6]. The averaged yaw angle suggests that the overall turning has not changed and thus the reduction in loss cannot be attributed to a change in overall loading.

8 BLADE SURFACE STATIC PRESSURE

Figures 7 and 8 show the static pressure distribution for the two blades. Note that the blade tapping radial positions are not identical but a comparison of the graphs allows the trends to be clearly determined.

The static pressure distribution for the C0 blade (Fig. 7) shows the 'flat topped' profile of the Durham cascade profile with the suction side pressure levelling off after ~ 35 per cent Cax. This
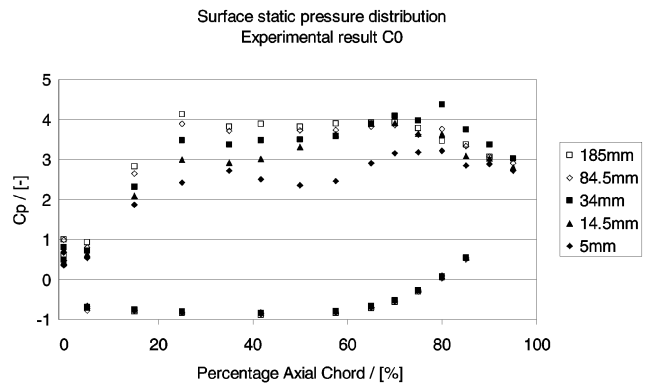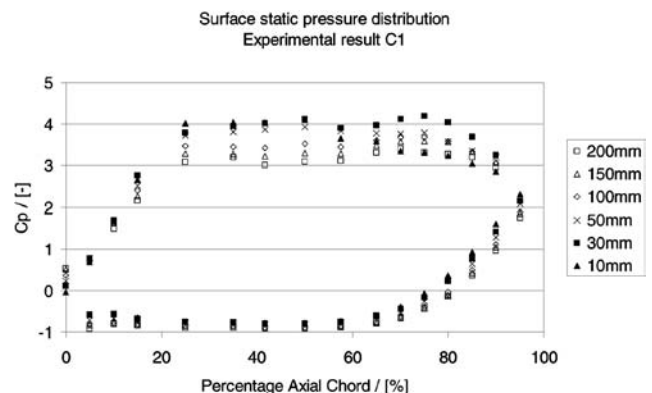

Fig. 7 Blade static pressures: C0 blade

may contrast with more recent aerofoil designs which tend to 'aft load' the blade. The prismatic blade shows a gradual SS diffusion as the end-wall is approached. The effect of the passage vortex can be seen in the increase in Cp value between 70–100 per cent Cax for the $r = 5$ and 15 mm tappings.

The C1 blade (Fig. 8), in contrast, shows a reduced loading at mid-span that increases as the end-wall is approached. The influence on the static pressure coefficient of the passage vortex at low radial heights is again apparent.
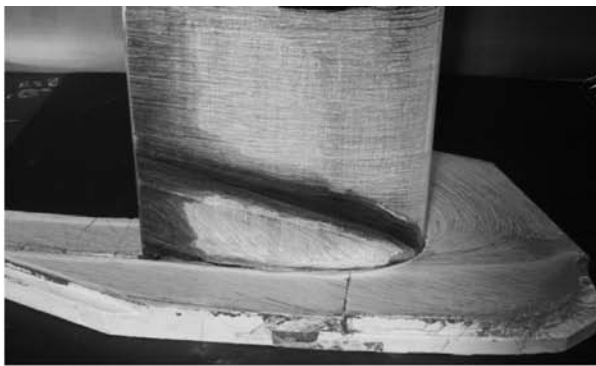
9 FLOW VISUALIZATION

A conventional oil and dye visualization technique was used; a yellow dye was applied to the blades and a red dye on the end-wall. The blade is coloured black and the end-wall is white; therefore, an absence of dye on the end-wall is a light colour, whereas on the blade, an absence of dye is a dark colour.
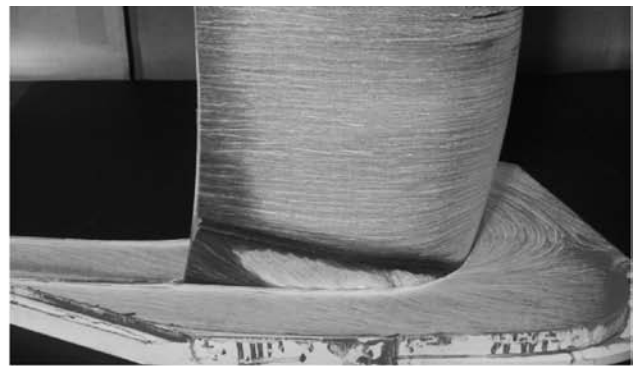
Figure 9 shows the suction side leg of the HSV and the passage vortex separation line climbing up the SS for both C0 and C1. At the trailing edge, the passage vortex for C1 appears to be much closer to the

Fig. 8 Blade static pressures: C1 blade

(a) Prismatic (C0) blade   (b) RCL (C1) blade

Fig. 9 Flow visualization: passage vortex growth

end-wall than the C0 case. However, such a great difference is not seen in the traverses 28 per cent Cax downstream of trailing edge, where the passage vortex cores are more similarly located.

Figure 10 provides details of the end-wall flow for C0 and C1. In Fig. 10(a), the SS leg and PS leg of the HSV are indicated for the prismatic blade. Comparison with Fig. 10(b) shows the shift of the SS HSV blade attachment point around the SS towards the trailing edge on C1. The end-wall trace of the pressure side leg of the HSV (seen close to the bottom of the image in Fig. 10(a) for C0 is not visible on C1.

10   DISCUSSION AND CONCLUSIONS

The effect of the RCL is shown to agree with that expected from the literature. At the end-wall, the radial component of blade force reduces the pressure causing a shift in flow towards the end-wall within the blade passage. As the flow leaves the trailing edge, the radial force is removed and so the flow redistributes towards mid-span. Thus in Fig. 9, the flow visualization shows the secondary flow for C1 confined closer to the end-wall, but at the traverse position 28 per cent Cax downstream, the location of the passage vortices and loss cores is very similar for C0 and C1.

The RCL also increases the loading near the end-wall as seen in the increased overturning with C1 and the blade static pressure distributions. There is a corresponding unloading at mid-span as shown by the reduction in turning at mid-span and again by the pressure distributions. However, the reduction in turning is compensated by the increased overturning near the end-wall, so that the overall turning is not significantly changed. The pitch-averaged loss (Fig. 5) shows an increase up to 70 mm from the end-wall. Beyond that there is a significant reduction in loss, so that overall the loss is reduced by 11 per cent with the RCL.

The reduction in mid-span turning and loss observed at the traverse position 28 per cent Cax
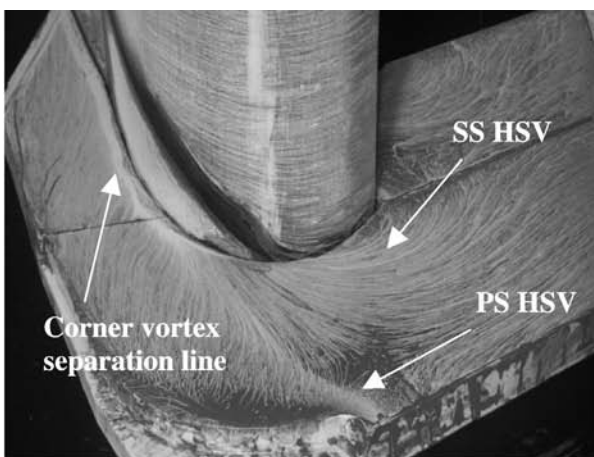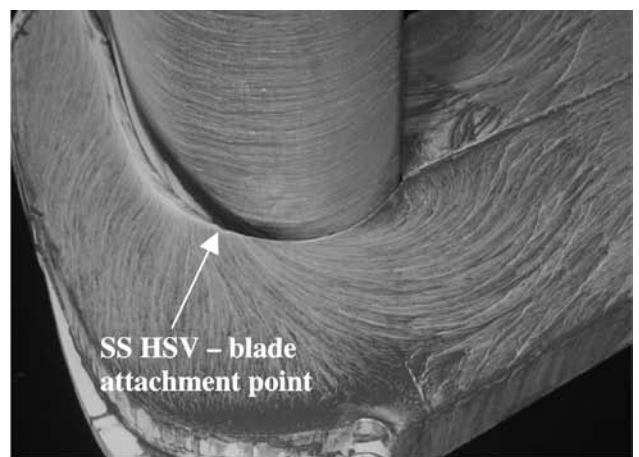
(a) Prismatic (C0) blade   (b) RCL (C1) blade

Fig. 10 Flow visualization: end-wall flow

downstream can be understood by considering the three-dimensional effects caused by the RCL. The stream tube is thickened as the axial velocity is reduced from leading to trailing edge in the blade passage, and the acceleration is therefore reduced. Thus, the blade surface velocities are reduced causing a reduction in frictional loss. At the trailing edge, the exit flow angle will be similar to the two-dimensional value, but as the stream tube is thinned downstream (with the flow redistribution) the axial velocity increases, whereas the tangential component of velocity is unchanged. Thus, the yaw angle is reduced as observed at the traverse position 28 per cent Cax downstream.

From the work presented in this paper, a number of specific conclusions can be drawn.

1. RCL reduces loss at the mid-span and increases it towards the end-wall.
2. The blade profile and loading given results in an overall decrease in loss of 11 per cent.
3. The mass-averaged turning angle remains the same for both cases, confirming that the RCL design has reduced loss while maintaining the same overall blade loading.
4. The exit yaw angle has become more nonuniform and this may result in increased downstream mixing loss.
5. The results are consistent with those found by other researchers.
6. An understanding of the effects of RCL requires an appreciation of the three-dimensional effects produced by the RCL.

ACKNOWLEDGEMENT

REFERENCES

1 **Harrison, S.** The influence of blade lean on turbine losses. ASME 90-GT-55, 1990.
2 **Ingram, G., Gregory-Smith, D. G.,** and **Harvey, N.** The benefits of turbine endwall profiling in a cascade. *Proc. Instn Mech. Engrs, Part A: J. Power and Energy*, 2005, **219**(A1), 49–60.
3 **Sharma, O., Kopper, F., Stetson, G., Magge, S., Price, F.,** and **Ni, R.** A perspective on the use of physical and numerical experiments in the advancement of design technology for axial flow turbines. In XVI International Symposium on *Air Breathing Engines (ISABE)*, Cleveland, OH, AIAA, Paper AIAA–2003–1035, 2003.
4 **Denton, J.** and **Xu, L.** The exploitation of three-dimensional flow in turbomachinery design. *Proc. Instn Mech. Engrs, Part C: J. Mechanical Engineering Science*, 1999, **213**, 125–137.
5 **Gregory-Smith, D. G.** Calculations of the secondary flow in a turbine cascade. In International Symposium on *Computational Fluid Dynamics in Aeropropulsion*, ASME International ME'95 Congress and Exposition, San Francisco, AD-Vol. 49, pp. 77–87, November, 1995.
6 **Ingram, G.** Endwall profiling for the reduction of secondary flow in turbines. PhD Thesis, University of Durham, 2003.

APPENDIX 1

Notation

Cax	axial chord
Cp0	total pressure coefficient; (upstream–local)/inlet dynamic head
Cp	static pressure coefficient; (upstream–local)/inlet dynamic head
C0	prismatic reference case blade
C1	reverse compound leaned blade
PS	pressure surface
RCL	reverse compound lean
r	span/height
SS	suction surface

APPENDIX 2: DEFINITION OF SECONDARY VECTORS

The secondary velocity at any position is obtained by resolving along and normal to the local mid-span flow direction at that pitchwise position. Thus, within the blade there may be a significant variation across the pitch for the reference angle. The plotted secondary vector is projected in the direction of the mid-span velocity onto the axial viewing plane as shown in Fig. 11.
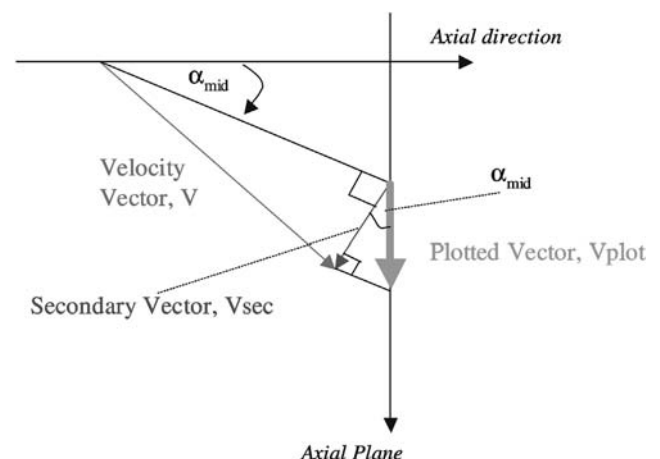

Fig. 11 Secondary velocity vectors